Modeling Microcapsules That Communicate through Nanoparticles To Undergo Self-Propelled Motion

O. Berk Usta, Alexander Alexeev,[†] Guangdong Zhu,[‡] and Anna C. Balazs*

Chemical Engineering Department, University of Pittsburgh, Pittsburgh, Pennsylvania 15261. [†]Current address: George W. Woodruff School of Mechanical Engineering, Georgia Institute of Technology, Atlanta, GA 30332-0405. [‡]Current address: Mechanical Engineering Department, University of New Mexico, Albuquerque, NM 87131.

ARTICLE

ABSTRACT Using simulation and theory, we demonstrate how nanoparticles can be harnessed to regulate the interaction between two initially stationary microcapsules on a surface and promote the self-propelled motion of these capsules along the substrate. The first microcapsule, the "signaling" capsule, encases nanoparticles, which diffuse from the interior of this carrier and into the surrounding solution; the second capsule is the "target" capsule, which is initially devoid of particles. Nanoparticles released from the signaling capsule modify the underlying substrate and thereby initiate the motion of the target capsule. The latter motion activates hydrodynamic interactions, which trigger the signaling capsule to follow the target. The continued release of the nanoparticles sustains the motion of both capsules. In effect, the system constitutes a synthetic analogue of biological cell signaling and our findings can shed light on fundamental physical forces that control interactions between cells. Our findings can also yield guidelines for manipulating the interactions of synthetic microcapsules in microfluidic devices.

KEYWORDS: self-propelled motion · microcapsules · nanoparticles · lattice Boltzmann model · computational modeling

Biological cells communicate through a complex chemical process where a signaling cell secretes molecules that are then detected by receptors on the target cell. This passage of information allows the cells to cooperate and thereby carry out a diverse range of functions. Herein, we use computational modeling and theory to design a synthetic system that effectively mimics this biological process. In particular, we show how one polymeric microcapsule "signals" to another and thereby initiates the motion of both. Microcapsules (such as those fabricated by the sequential deposition of oppositely charged chains[1]) provide optimal features for performing this biomimetic behavior: they encompass a porous shell and a fluid-filled core, which can contain nanoparticles.[2] As encapsulated nanoparticles diffuse through the porous shell and into the surrounding fluid, they act as signaling species and the capsule can be viewed as secreting the vital compounds. In our scenario, both the signaling and the target microcapsules sit on an initially homogeneous adhesive surface. Neither capsule alone can move along this surface; however, the nanoparticle-facilitated communication between the two promotes and sustains collective, directed motion.

While researchers have focused on isolating factors that promote the self-directed motion of individual liquid droplets,[3–15] there have been few studies to examine how collective behavior between droplets[16] or capsules can lead to self-propelled movement. Our findings can provide insight into fundamental physical processes that control chemotaxis between biological cells.[17] In addition, polymeric capsules are finding use as microreactors and the results yield guidelines for manipulating their interactions in microfluidic devices.

Using a novel computational approach (see Methods), we simulate the behavior of the system shown in Figure 1; the first capsule (the signaling capsule) contains dispersed nanoparticles in its fluid-filled core, while the second fluid-filled capsule (the target capsule) is initially devoid of nanoparticles. Each capsule's two-dimensional, rigid shell is composed of two layers of lattice nodes, which make up the inner and outer surfaces. We assume that the nanoparticles can diffuse through this shell,[18] but the fluid content of the capsule remains constant. The released nanoparticles can chemisorb onto the substrate and the adsorbed nanoparticles modify the wetting properties of the surface.[19] In particular, the strength of the adhesive interaction between the capsules and surface decreases with the fractional surface coverage of nanoparticles. The adsorbing nanoparticles can thereby create an adhesion gradient along the surface, and if the gradient is sufficiently asymmetric,[3–16] a capsule could be driven by enthalpic forces to move from

*Address correspondence to balazs1@engr.pitt.edu.

Received for review November 20, 2007 and accepted January 26, 2008.

Published online February 28, 2008.
10.1021/nn700379v CCC: $40.75

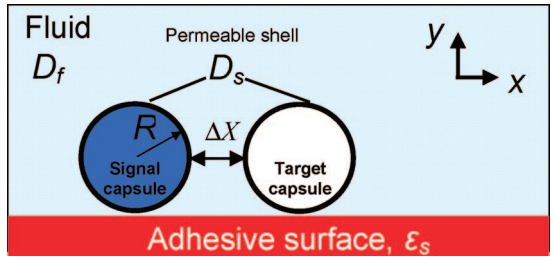

Figure 1. Schematic of the system: two capsules with radii $R = 12.5$ and shell thickness of $h \approx 1.3$ are separated by an initial distance ΔX on a surface with an initially uniform adhesive strength $\epsilon_s = \epsilon$. The signaling capsule contains $N = 2 \times 10^5$ nanoparticles, which are released at $t = 0$. The fluid has a viscosity of $\nu = 1/6$ and density of $\rho = 1$. The size of the simulation box is $L_x = 300$ and $L_y = 60$ and periodic boundary conditions are applied in the lateral direction. The dimensions are given in LB units.

a less adhesive area to a more "sticky" portion (*i.e.*, lower particle surface coverage).

RESULTS AND DISCUSSION

Panels a−c of Figure 2 show the scenario in the case of a single signaling capsule on the surface. The blue dots mark the nanoparticles, showing the species that are still encapsulated and those that have diffused into the surrounding solution. Some fraction of the nanoparticles has adsorbed onto the surface and modified the adhesive interaction between the capsule and this substrate. The red line below the surface indicates the adhesion profile due to the deposited particles. Since these particles are simply undergoing Brownian motion, the particle deposition and the resulting adhesion profile are symmetric about the capsule's center. Thus, there is no driving force for the single signaling capsule to move and consequently, the capsule remains fixed in space.[20]

The introduction of the empty target capsule, however, breaks the symmetry in the system. The signaling capsule produces an asymmetric concentration profile of nanoparticles around the target capsule's center of mass, with more particles being localized between the two capsules than on the far side of the target capsule (Figure 2, panels d−f). This asymmetry leads to an adhesion gradient around the target capsule and, consequently, a net driving force that propels the target capsule away from the signaling capsule, *i.e.*, toward the higher adhesion. In other words, it is the asymmetry in the adhesion gradient that initiates the movement of the target capsule. Once the target capsule moves, it sets additional forces into play. In particular, recall that the target capsule is not traveling in a vacuum but, rather, moving through a viscous fluid, which mediates its motion. These hydrodynamic interactions give rise to a net force[21] on the signaling capsule that drives it to follow the target capsule. Therefore, the presence of the second capsule results in the motion of both.

While hydrodynamic interactions between the two capsules play a crucial role in initiating the motion of the signaling capsule, these interactions alone cannot lead to sustained motion. For both capsules to keep moving, the signaling capsule must also be driven by a gradient in the surface coverage. The following variables play a key role in our system: the diffusion of the nanoparticles in fluid, D_f, diffusion of particles through the capsule's shell, D_s, the initial adhesion, ϵ, and the surface saturation concentration, C_{max} (*i.e.*, the maximum number of nanoparticles that can chemisorb per unit area of surface). Herein, we fixed D_f (note that $D_s \ll D_f$ throughout[22]) and examined the effect of the other parameters on the behavior of the system.

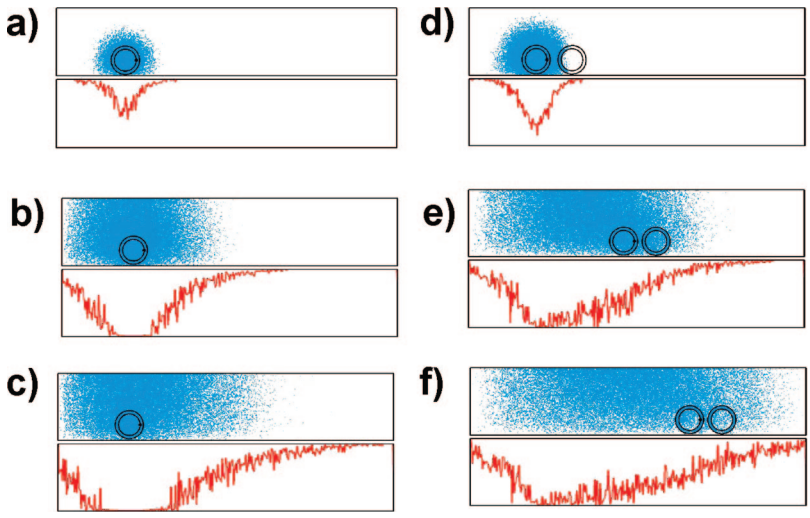

Figure 2. Snapshots of a single capsule and two capsules on an adhesive substrate. The initial conditions are identical for both simulations: $D_f = 0.01$, $D_s = 0.0002$, $\epsilon = 0.01$, $C_{max} = 200$. The signaling capsule releases nanoparticles (in blue), which deposit on the surface and produce the adhesion profile shown in red. (a−c) Due to the symmetry of the adhesion profile, the single capsule remains stationary. (d−f) The target capsule sits on an asymmetric adhesion profile, which results in a net force driving the target capsule away from the signal capsule. Once the target capsule starts moving, it displaces the surrounding fluid, which drags the signaling capsule. Thus, the hydrodynamic interaction initiates motion of the signaling capsule, which is then sustained by the adhesion gradient.

To simplify the discussion, we specify the velocity of the signal capsule as V_{caps} and the speed at which the gradient propagates across the surface as V_{grad}. The capsule velocity V_{caps} is dictated primarily by the mobility of the capsule in solution, μ, the adhesive strength, ϵ, and the gradient in the surface concentration. The mobility is defined as $\mu = (6\pi R\ \nu\rho)^{-1}$ where R is capsule radius and ρ is the density of the host fluid. On the other hand, the propagation of the surface gradient is dictated primarily by D_s (since $D_s \ll D_f$, the diffusion through the shell controls the release rate of nanoparticles and, in turn, the rate at which the surface is modified). The ratio of V_{caps} and V_{grad} can be characterized by the dimensionless number $\theta = \mu\epsilon/D_s$. Below, we discuss our results in terms

of θ, the maximum surface saturation concentration, C_{max}, and the initial distance between the capsules, Δx.

We first consider the case of "arrested" motion (see Figures 3a and 4), where the signaling capsule moves slower than the propagation of the concentration profile, or $V_{caps} < V_{grad}$. This behavior occurs for any of the following conditions: $\Delta x \geq R$, which leads to a weak initial perturbation through hydrodynamic interactions; θ is relatively low and C_{max} is relatively low. The values of θ and C_{max} that give rise to "arrested" motion are shown in Figure 4. Low θ is possible with either a high D_s or low ϵ. When the diffusion coefficient is too high, the rate at which the particles modify the surface is sufficiently rapid that the adhesion gradient propagates too quickly for the signaling capsule to get onto this heterogeneous region. When the adhesion strength is too low, the driving force for the capsules is too small to achieve a sufficiently high velocity to follow the propagating adhesion gradient. Similarly, if C_{max} is relatively low, the coverage of the surface by nanoparticles happens too rapidly for the signaling capsule to reach the gradient. Therefore, we observe that the signaling capsule eventually sits on a surface with full surface coverage and no gradient. In other words, in the center of mass frame of the signaling capsule, we see an advancing concentration profile (see Figures 3a and 5a).

A transition from arrested motion ($V_{caps} < V_{grad}$) to sustained motion ($V_{caps} \geq V_{grad}$) is achieved when either θ or C_{max} is increased (with all other parameters held fixed) (see Figure 4). An increase in θ occurs either by a decrease in D_s or an increase in the initial adhesion strength, ϵ. In this case, we observe that both capsules move roughly at the same speed (Figure 3b,c) and the distance between capsules is constant after an initial rearrangement. When the capsules and the concentration profile evolve at the same speed, $V_{caps} = V_{grad}$, we see that the concentration profile is stationary in the center of mass frame of the signaling capsules (Figures 3a and 5b) and the capsules experience a constant driving force, resulting in a relatively constant velocity.

A second scenario for sustained motion occurs when both the adhesion coefficient ϵ and C_{max} are sufficiently high that the capsules initially move faster than the propagation of the gradient, $V_{caps} > V_{grad}$. In this case, the target capsule can reach the edge of the concentration profile and slow down both particles while the signaling particle is still on a strong adhesion gradient. The released nanoparticles, however, create a new gradient, which causes the capsules to speed up. This cycle repeats and results in an oscillatory velocity for both the capsules and the concentration profile (Figure 3c). In Figure 4, we summarize the effects of each parameter and clearly illustrate the transition from arrested to sustained motion of a two-capsule system.

To verify the above observations, we examine a simpler system. Here, a single point source emits nanoparticles and moves on the surface with a velocity that depends on the adhesion strength and the gradient in the cumulative flux of nanoparticles at the substrate. In panels a and b of Figure 5, we plot the nanoparticle flux profile, through the boundary, in the moving frame of the center of mass of the source at different times. Figure 5a shows that for the case of arrested motion, the source eventually sits on a surface of zero gradient and that the profile moves away from the source, as seen in our simulations. However, in the case of sus-

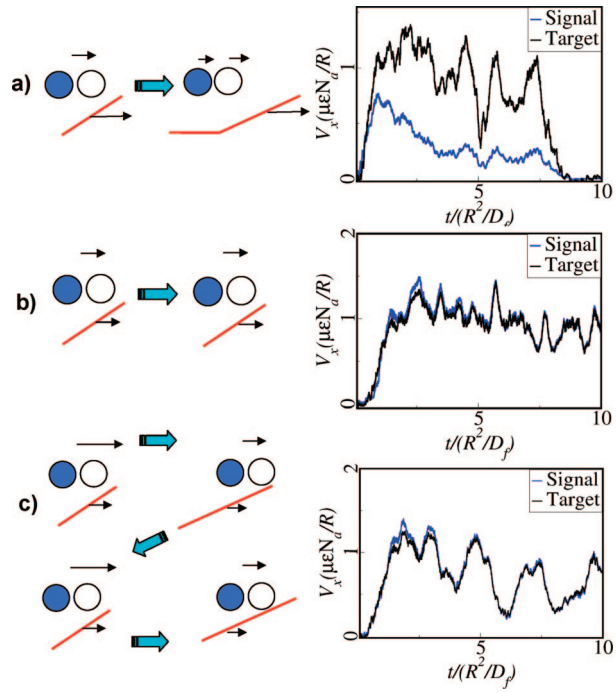

Figure 3. Different regimes of behavior in the system. In the schematic images on the left, the signaling capsule is drawn in blue, the target capsule is drawn in white, and the red line illustrates the position of the gradient. The right column shows the velocity evolution for the signaling and target capsules. Here N_a is the number of surface nodes that interact with the adhesive surface. (a) Arrested motion: the adhesion gradient propagates too rapidly so the capsules end up on a surface with no gradient and stop ($V_{caps} < V_{grad}$, $D_f = 0.01$, $D_s = 0.0006$, $\epsilon = 0.01$, $C_{max} = 100$). (b) Sustained motion: the capsules and the gradient propagate with roughly the same velocity ($V_{caps} \approx V_{grad}$, $D_f = 0.01$, $D_s = 0.0002$, $\epsilon = 0.01$, $C_{max} = 200$). (c) Oscillatory motion: initially the capsules move faster than the gradient, resulting in periodic velocity changes for both the capsules ($V_{caps} > V_{grad}$, $D_f = 0.01$, $D_s = 0.0006$, $\epsilon = 0.01$, $C_{max} = 300$).

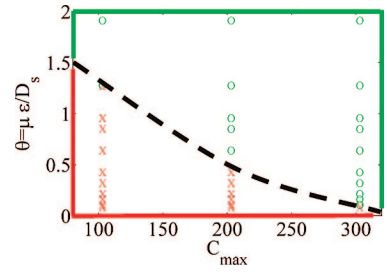

Figure 4. Phase map delineating the different regimes: "X" is for the arrested motion of the capsules, while "O" signifies the sustained motion. The dashed line shows the approximate boundary between these two regimes. In these calculations, we fixed $D_f = 0.01$.

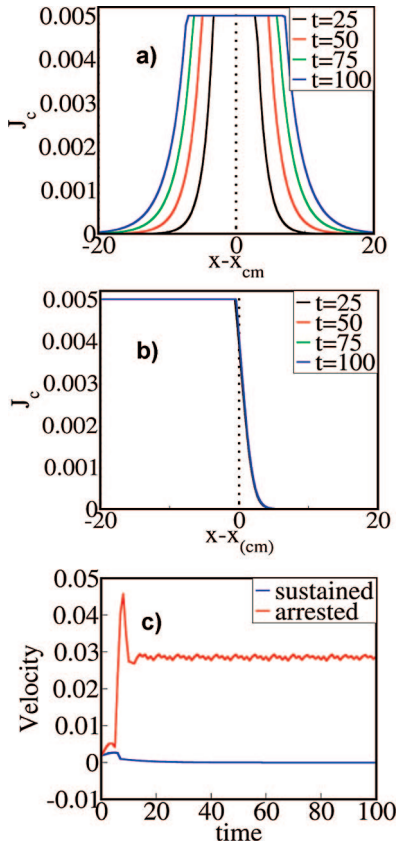

Figure 5. Results from the simplified theoretical model. Profiles of the nanoparticles flux through the substrate for (a) arrested motion and (b) sustained motion. The profiles are shown in the frame of the source's center of mass. Note that for (b), the plots for different times all overlap and fall onto one curve. (c) The velocities for the arrested ($y_0 = 2$, $D_0 = 0.02$, $\beta = 4$, $V = 0.002$) and sustained motion ($y_0 = 2$, $D_0 = 0.02$, $\beta = 16$, $V = 0.002$).

tained motion, we see (Figure 5b) a stationary flux profile in the center of mass frame of the source, demonstrating that the source and the concentration profile move with the same velocity.

Through this simplified model, we find that the point source can undergo sustained motion, in qualitative agreement with the simulation (case 2 in Figure 3).[23] Figure 5c shows that by simply decreasing the adhesion strength at the surface or the mobility of the point source, the system can undergo a transition from sustained movement to arrested motion, again in agreement with the simulation. Furthermore, as we noted above, decreasing D_0 can lead to sustained motion, while increasing this parameter leads to arrested motion. Again, the controlling factor is the competition between the advancing of the concentration profile and the capsule motion as described by the dimensionless number θ.

CONCLUSIONS

In summary, we have designed a simple biomimetic system where two synthetic capsules can effectively communicate with each other through the released nanoparticles and thereby move together along the substrate. The system also exhibits an interesting form of chemotaxis that has been recently observed in biological cells;[17] namely, our signaling capsule can both send directional cues (*via* the nanoparticles) and receive directional cues (through the hydrodynamic interactions with the target capsule). The findings indicate that hydrodynamic interactions could play an important role in the sensing and signaling behavior of biological cells. While the results presented herein were generated from two-dimensional simulations, the system could be experimentally realized by placing capsules on an attractive stripe on a substrate or within a narrow channel.

METHODS

The dynamics of the host and encapsulated fluids is captured through the lattice Boltzmann model (LBM),[24] which is an efficient solver for the Navier–Stokes equation. The host and internal fluids interact with the solid shells through appropriate boundary conditions.[25,26] In particular, the shell imposes its momentum on the surrounding fluids through the corresponding velocity distributions in the LBM. In turn, the capsules experience forces due to the fluid pressure and viscous stresses at the interfaces.

We integrate the above approach with a Brownian dynamics model for the nanoparticles to simulate the diffusion of the particles from the interior of the fluid-filled capsule through the shell to the host solution. In particular, at the start of the simulation, a fixed number of nanoparticles is introduced into the fluid-filled interior of the microcapsule. The nanoparticles are modeled as point particles whose trajectories obey the following stochastic differential equation:[27,28]

$$d\mathbf{r}(t) = \mathbf{u}(\mathbf{r}, t)\, dt + \sqrt{2D_0}\, d\mathbf{W}(t)$$

The first term gives the advection due to the local fluid velocity $\mathbf{u}(\mathbf{r},t)$. Note that $\mathbf{u}(\mathbf{r},t) = 0$ until the target capsule is driven into motion (by the asymmetric adhesion gradient); once the target moves, it induces a flow field, making $\mathbf{u}(\mathbf{r},t) \neq 0$. The second term in the above expression is the Brownian contribution, with D_0 being the particles' diffusion coefficient and $d\mathbf{W}(t)$ being the differential of a Wiener process with unit variance. Within the fluid, $D_0 = D_f$ and within the microcapsule's shell, the particles have an effective diffusion coefficient $D_0 = D_s$. Given that ν is the kinematic viscosity of the host fluid, the Schmidt number, $Sc = \nu/D_f$, for our simulations lies between 10 and 20, in the range of typical values for nanoparticle filled fluids.[29] The encapsulated and external fluids are taken to be identical single-component liquids, which have the same viscosity and density. We neglect interactions between the nanoparticles; this approximation is appropriate for nanoscopic particles at a relatively low concentration.[30] The entire system operates in the low-Reynolds-number regime, where inertial effects can be neglected.

Nanoparticles that diffuse from the interior of the "signaling" capsule can chemisorb onto the substrate (see Figure 1); this behavior is simulated by implementing the following general mass transfer boundary conditions:

$$-D_0 \mathbf{n} \cdot \nabla c\Big|_{\text{surface}} = f(c_s)$$

where **n** is the unit normal to the surface, $\nabla c_{surface}$ is the gradient in the particle concentration at the surface, and $f(c_s)$ is the flux of particles that enter or leave the fluid (with $f < 0$ for particle deposition). To the lowest order, $f(c_s)$ can be modeled by a linear kinetic law:[31]

$$f(c_s) = -k(1 - \Theta)c_s$$

where $\Theta(\mathbf{r},t)$ is the fractional coverage of the surface by the nanoparticles. Here, the reaction rate is proportional to the concentration of nanoparticles at the surface, c_s, with the proportionality constant being the product of a reaction constant k and the fraction $(1 - \Theta(\mathbf{r},t))$ of the surface area that is "empty" or "available" to the nanoparticles. The maximum number of nanoparticles that can chemisorb *per unit area of surface* is controlled by the parameter C_{max}, which we vary in our simulations; in effect, C_{max} is a measure of the reactivity of the surface. (Note that $\Theta = c_s/C_{max}$.)

The interaction between the capsules and this surface is modeled *via* a nonspecific Morse potential

$$\varphi(r) = \epsilon_s\left(1 - \exp\left[-\frac{(r - r_0)}{\kappa}\right]\right)^2$$

where ϵ_s and κ characterize the respective strength and range of the interaction potential. Additionally, r represents the distance between nodes on the capsule's outer surface and the substrate, which is also composed of lattice nodes, and r_0 is the distance where this force equals zero. We set $\kappa = 1$ and $r_0 = 1$, while ϵ_s depends on the nanoparticle surface coverage. We assume that the adsorbed nanoparticles modify the wetting properties of the surface and, specifically, that the strength of the adhesive interaction decreases with the fractional surface coverage, *i.e.*, $\epsilon_s = \epsilon(1 - \Theta)$, with ϵ being the initial adhesive strength of the surface.

We validate the observations from the simulations by using a simpler system where a single point source emits nanoparticles. The point source moves along the surface with a velocity that depends on the adhesion strength and the gradient in the cumulative flux of nanoparticles at the substrate. The point source's motion is in the overdamped regime (where inertia is neglected), and thus, the velocity of the source, $\dot{x}_0$, is directly proportional to the gradient of the cumulative flux through the substrate, J_c, at the position of the source, x_0:

$$\dot{x}_0 = \beta \nabla J_c(x_0) + Ve^{-t/t_c} \quad (1)$$

The proportionality constant β lumps together the surface adhesion strength and mobility of the source. To provide the asymmetry in the absence of a second capsule, the point source is "kicked" into motion with an initial velocity V, which decays with a characteristic time of t_c.

To calculate the flux on a boundary (x, $y = 0$), given a source at (x_0, y_0), we use the flux expression with boundary conditions for a perfectly adsorbing wall. This expression is based on the infinite space Green's function for a source and an image system with two bounding surfaces set apart by a height H. With a point source emitting N particles at each interval Δt, the flux at the boundary for a period Δt is given by the following equation[32]

$$j_{y,0}(x, \Delta t) = \frac{N}{4\pi D_0 \Delta t^2} e^{-(x - x_0(t))^2/4D_0\Delta t} \times \sum_{n=-\infty}^{n=\infty} (y_0 + 2nH) e^{-(y_0 + 2nH)^2/4D_0\Delta t} \quad (2)$$

Here, we limit n to 1 so that we only account for the first two images. To calculate the cumulative flux at an arbitrary time t, we integrate over time, while updating the position of the source:

$$J_c(x, t) = \int_0^t \frac{N}{4\pi D_0(t - \tau)^2} e^{-(x - x_0(\tau))^2/4D_0(t-\tau)} \times \sum_{n=-1}^{n=1} (y_0 + 2nH) e^{-(y_0 + 2nH)^2/4D_0(t-\tau)} d\tau \quad (3)$$

The motion of the source is inherent in this calculation since x_0, in eq 3, is time dependent and is updated by the equation of motion (eq 1). We solve numerically the coupled eqs 1 and 3 and track the trajectory and velocity of the source and the nanoparticle flux profiles. We apply a cutoff value, $J_{C_{max}}$, at each location to mimic varying the saturation concentration, C_{max}, in the simulations.

Acknowledgment. The authors gratefully acknowledge financial support from DOE (A.A. and G.Z.) and ONR (O.B.U.).

REFERENCES AND NOTES

1. Peyratout, C. S.; Dahne, L. Tailor-Made Polyelectrolyte Microcapsules: From Multilayers to Smart Containers. *Angew. Chem., Int. Ed.* **2004**, *43*, 3762–3783.
2. Skirtach, A. G.; Dejugnat, C.; Braun, D.; Susha, A. S.; Rogach, A. L.; Parak, W. J.; Mohwald, H.; Sukhorukov, G. B. The Role of Metal Nanoparticles in Remote Release of Encapsulated Materials. *Nano Lett.* **2005**, *5*, 1371–1377.
3. Brochard, F. Motions of Droplets on Solid Surfaces Induced by Chemical or Thermal Gradients. *Langmuir* **1989**, *5*, 432–438.
4. Ichimura, K.; Oh, S.-K.; Nakagawa, M. Light-Driven Motion of Liquids on a Photoresponsive Surface. *Science* **2000**, *288*, 1624–1626.
5. Len, M. P.; Uwe, T. Asympototic Theory for a Moving Droplet Driven by a Wettability Gradient. *Phys. Fluids* **2006**, *18*, 042104–042113.
6. Thiele, U.; John, K.; Bar, M. Dynamical Model for Chemically Driven Running Droplets. *Phys. Rev. Lett.* **2004**, *93*, 027802–027805.
7. Yochelis, A.; Pismen, L. M. Droplet Motion Driven by Surface Freezing or Melting: A Mesoscopic Hydrodynamic Approach. *Phys. Rev. E* **2005**, *72*, 025301–025304.
8. Dos Santos, F. D.; Ondarçuhu, T. Free-Running Droplets. *Phys. Rev. Lett.* **1995**, *75*, 2972–2977.
9. Chaudhury, M. K.; Whitesides, G. M. Hot to Make Water Run Uphill. *Science* **1992**, *256*, 1539–1541.
10. Sandre, O.; Gorre-Talini, L.; Ajdari, A.; Prost, J.; Silberzan, P. Moving Droplets on Asymmetrically Structured Surfaces. *Phys. Rev. E* **1999**, *60*, 2964–2972.
11. de Gennes, P. G. Running Droplets in a Random Medium. *C. R. Acad. Sci., Ser. IIb: Mec., Phys., Astron.* **1999**, *327*, 147–154.
12. Linke, H.; Aleman, B. J.; Melling, L. D.; Taormina, M. J.; Francis, M. J.; Dow-Hygelund, C. C.; Narayanan, V.; Taylor, R. P.; Stout, A. Self-Propelled Leidenfrost Droplets. *Phys. Rev. Lett.* **2006**, *96*, 154502–154505.
13. John, K.; Bar, M.; Thiele, U. Self-Propelled Running Droplets on Solid Substrates Driven by Chemical Reactions. *Eur. Phys. J. E* **2005**, *18*, 183–199.
14. Sumino, Y.; Magome, N.; Hamada, T.; Yoshikawa, K. Self-Running Droplet: Emergence of Regular Motion from Nonequilibrium Noise. *Phys. Rev. Lett.* **2005**, *94*, 068301–068304.
15. Lee, S.-W.; Kwok, D. Y.; Laibinis, P. E. Chemical Influences of Absorption-Medicated Self-Propelled Drop Movement. *Phys. Rev. E* **2002**, *65*, 051602–051610.
16. Nakata, S.; Komoto, H.; Hayashi, K.; Menzinger, M. Mercury Drop "Attacks" an Oxidant Crystal. *J. Phys. Chem. B* **2000**, *104*, 3589–3593.
17. Shields, J. D.; Fleury, M. E.; Yong, C.; Tomei, A. A.; Randolph, G. J.; Swartz, M. A. Autologous Chemotaxis as a Mechanism of Tumor Cell Homing to Lymphatics via Interstitial Flow and Autocrine CCR7 Signaling. *Cancer Cell* **2007**, *11*, 526–538.
18. We note that the permeability of microcapsules formed from the layer-by-layer (LbL) deposition of oppositely

charged chains can be controlled experimentally by varying, for example, the pH or salt concentration of the solution, as detailed in ref [1].
19. Here, we focus on nanoparticles as the encapsulated species that modify the surface properties upon release from the capsule. We anticipate, however, that surfactants could also be harnessed for this purpose. The concentration of surfactants in the solution should ideally be below the critical micelle concentration (cmc) so that the species bind to the surface rather than forming micelles in solution. This can, however, be controlled by tailoring the permeability of the capsule's shell so that the surfactant concentration in solution is relatively low.
20. Sufficiently strong adhesion fluctuations due to an uneven deposition of nanoparticles might provoke a spontaneous motion of a single capsule in a random direction. Here, however, we consider regimes where the viscous forces on the capsule are sufficiently strong to prevent this scenario.
21. Espanol, P. On the Propogation of Hydrodynamic Interactions. *Physica A* **1995**, *214*, 185–206.
22. This is a reasonable assumption since the diffusivity of the nanoparticles in a simple fluid (D_f) is expected to be greater than that through a porous polymeric shell (D_s).
23. This simplified model does not yield oscillatory motion (case 3 in Figure 4) since the presence of the second (target) capsule seems to be critical to producing this behavior.
24. Succi, S., *The Lattice Boltzmann Equation for Fluid Dynamics and beyond*. Oxford University Press: Oxford, 2001; p xvi.
25. Alexeev, A.; Verberg, R.; Balazs, A. C. Modeling the Motion of Microcapsules on Compliant Polymeric Surfaces. *Macromolecules* **2005**, *38*, 10244–10260.
26. Bouzidi, M.; Firdaouss, M.; Lallemand, P. Momentum Transfer of a Boltzmann-Lattice Fluid with Boundaries. *Phys. Fluids* **2001**, *13*, 3452–3459.
27. Ottinger, H. C. *Stochastic Processes in Polymeric Fluids*. Springer-Verlag: Berlin, 1996; p 362.
28. Verberg, R.; Yeomans, J. M.; Balazs, A. C. Modeling the Flow of Fluid/Particle Mixtures in Microchannels: Encapsulating Nanoparticles within Monodisperse Droplets. *J. Chem. Phys.* **2005**, *123*, 224706(9).
29. Garrick, S. C.; Lehtinen, K. E. J.; Zachariah, M. R. Nanoparticle Coagulation via a Navier-Stokes/Nodal Methodology: Evolution of the Particle Field. *J. Aerosol Sci.* **2006**, *37*, 555–576.
30. The assumption is also reasonable given that nanoparticles are typically coated with steric stabilizers to improve their solubility in the solution. The steric stabilizers also inhibit the particles from interacting.
31. Szymczak, P.; Ladd, A. J. C. Stochastic Boundary Conditions to the Convection-Diffusion Equation Including Chemical Reactions at Solid Surfaces. *Phys. Rev. E* **2004**, *69*, 036704–036712.
32. Verberg, R.; Alexeev, A.; Balazs, A. C. Modeling the Release of Nanoparticles from Mobile Microcapsules. *J. Chem. Phys.* **2006**, *125*, 224712–224721.